Thermal Integral Micro-Generation Systems for Solar and Conventional Use

Abraham Kribus
Environmental Sciences and Energy Research Department,
Weizmann Institute of Science,
Rehovot 76100, Israel
e-mail: avi.kribus@weizmann.ac.il

Thermal Integral Micro-Generation (TIMGen) systems on the scale of a few Watts are proposed for use with solar or fuel-derived heat. The optics, the thermal receiver, and several alternative generation technologies, including MEMS heat engines (Stirling and Brayton cycles), thermal photovoltaics, and thermoelectric, are discussed. Analysis of system performance shows the potential for efficiency comparable to photovoltaic cells and large-scale thermal plants. A major advantage of thermal systems over PV cells is the possibility of hybrid operation, both with sunlight and with another heat source when sunlight is not available. The alternative heat source can be another renewable or conventional fossil fuel. TIMGen plants compared to large-scale centralized thermal plants offer the advantages of modularity, scalability, redundancy and low cost via mass production. They can prove to be a very attractive option both for remote, self-contained electricity generation, and as an alternative to large-scale centralized plants.
[DOI: 10.1115/1.1464879]

1 Introduction

Solar thermal electricity generation systems have been proposed over a wide range of sizes, from a few kilowatts to hundreds of Megawatts [1]. Conventional power generation is also done in this wide range of sizes. The generation in both cases is centralized, performed by a single central engine or a small number of relatively large engines in parallel. In the solar plant case, the solar radiation is collected over a large area and the energy is then channeled to the central generation site. The central engine is usually made as large as possible, since this enables higher conversion efficiency. The centralized approach entails major challenges in distribution, redundancy, and adjustment of electricity production rate to match demand. For solar thermal plants, not being yet a mainstream technology, the centralized approach is problematic in the transition from research and development to commercial applications. Centralized solar power plants are expected to become competitive when they reach the scale of 100 MW_e [2], since mass production of critical components requires high production volume. The investment and the risk associated with such large plants are very high, and attempts to commercialize these technologies have met with little success so far.

A diametrically opposite approach to thermal conversion is to consider the smaller scale rather than the larger scale. Thermal generators on the scale of a few Watts are proposed. A plant can have thousands or even millions of small, self-contained micro-generators. The possible advantages of this approach are:

- Unprecedented scalability to any desired size with no effect on performance (assuming that issues of connectivity, distribution, etc. can be resolved)
- High reliability due to massive redundancy (assuming that the individual generators are highly reliable)
- Low cost through mass production even for relatively low power levels
- Low investment and low risk in development and demonstration of the technology.

Recent developments in Micro-Electro-Mechanical System (MEMS) indicate that small-scale heat engines with built-in electricity generators are becoming feasible [3]. Additional options for direct thermal generation without a mechanical engine are also available. Four options are discussed in this paper: Brayton and Stirling heat engines, thermoelectric and thermophotovoltaic conversion. Downscaling the concentration optics is clearly feasible [4]. The only component whose downscaling cannot be deduced from previous work is the solar receiver. A receiver concept adapted for micro-generators is proposed and analyzed here. A complete Solar Thermal Integral Micro-Generator (STIMGen) system is then presented. A fuel-based Thermal Integral Micro-Generator (TIMGen), which is derived from the same principles by removing the solar part, is also discussed.

The STIMGens proposed here are similar in scale to photovoltaic cells. However, they are based on thermal conversion, which allows hybridization (operation with both solar heat and fuel) to continue generating electricity even when sunlight is not available. The external heat source can be conventional fuel, but a renewable source can also be used, for example, biogas derived from organic waste. This is a major advantage since it enables operation according to the actual demand for electricity, without limitation to sunlight hours only. This also permits stand-alone operation of a remote solar generator without reliance on a grid connection, without a conventional backup generator, and without the need for batteries.

In this paper, we consider the feasibility of this approach. First, the system components are presented: optics, thermal receiver, and generator subsystem. Next, the overall conversion efficiency of a complete solar micro-generator is estimated. Finally, an overview of possible applications and a comparison to other generating options are presented.

2 System Description

2.1 Optics. Concentrators are scalable practically to any desired size. On the scale of interest to STIMGen, a parabolic dish of 1 m diameter can collect about 630 W of radiation power (under insolation of 800 $W\,m^{-2}$), and concentrate most of it on a target of about 20 mm diameter. Several concentrators can be mounted on a common platform that tracks the sun [4,5]. Previous proposals for small concentrators intended to collect the light from each small dish into an optical fiber. All fibers are channeled to a central site, where the concentrated sunlight is absorbed and converted using conventional large-scale receiver and heat engine.

Contributed by the Solar Energy Division of THE AMERICAN SOCIETY OF MECHANICAL ENGINEERS for publication in the ASME JOURNAL OF SOLAR ENERGY ENGINEERING. Manuscript received by the ASME Solar Energy Division, October 2000; final revision, November 2001. Associate Editor: T. Mancini.

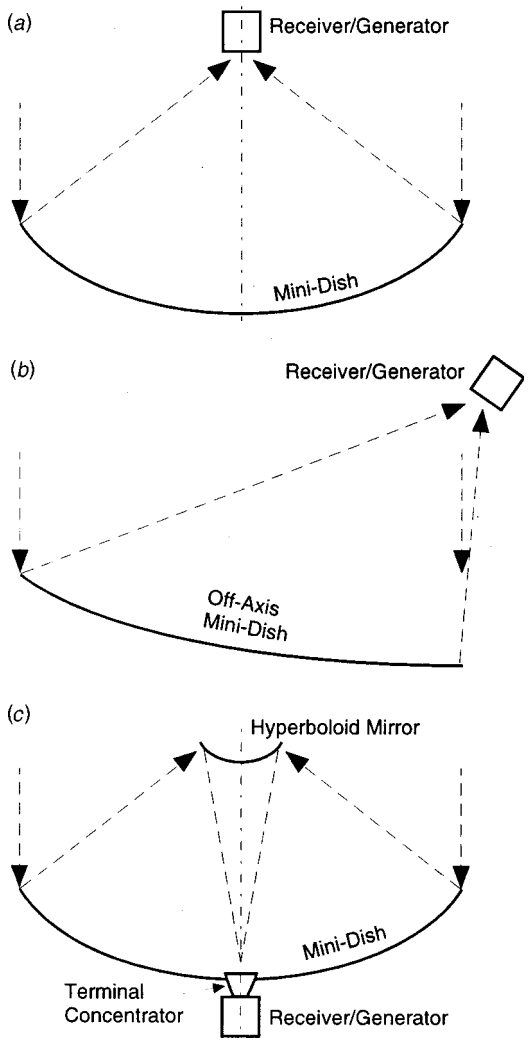

Fig. 1 Options for Mini-Dish concentrator: *a*) Receiver installed in the primary focus; *b*) An off-axis dish; *c*) Cassegrainian; the light is folded by a hyperboloidal reflector and reconcentrated by a terminal non-imaging concentrator.

The need to guide concentrated sunlight over long distances can make this approach expensive due to the cost of the fibers, and inefficient due to attenuation loss in the fibers [6,7]. However, in a STIMGen, the receiver and generator are local to the dish and no additional optical transport is needed. Manufacturing of small parabolic dishes should be simpler than large dishes or heliostats that require a large, stiff structure and alignment of many segments to a common curvature. If the STIMGen dishes are small enough to be produced in a single piece, they can be easily adapted for mass production, for example as done for automotive headlight reflectors. Issues of geometric accuracy and long-term durability will have to be addressed in such designs for mass production.

Several options for optical design are shown in Fig. 1. The simplest configuration, Fig. 1*a*, is to place the receiver/generator in the focal area of the mini-dish. This will block some of the incident radiation, especially if the heat rejection elements (Section 2.3) have to be large. This shading can be avoided if an off-axis dish is used, as shown in Fig. 1*b*. An off-axis dish will have somewhat larger area for the same collected power, leading to some penalty in efficiency. An alternative solution is to place the receiver behind the dish using Cassegrainian optics, Fig. 1*c*. This design involves a penalty in efficiency due to additional reflections, and in cost due to additional optical elements. The selection of the best trade-off between these considerations should be left to the detailed design of a system.

For the analysis in this paper, the simpler design of Fig. 1*a* was used with the receiver placed in the focal point of the dish. The dish was chosen to have a rim angle of $\theta_R = 45°$, providing a reasonably high concentration without the need to reject much low-flux radiation at the periphery of the focal region. The flux distribution at the focal plane was simulated using statistical ray tracing, using a limb-darkened sunshape model [1] with 5 mrad width, and reflector beam quality of 3 mrad representing typical surface and tracking errors. The intercept diameter d was determined as the largest diameter where the incident flux is larger than the thermal emission flux at the receiver wall temperature. This diameter determines the intercept efficiency:

$$\eta_{INT} = \frac{\int_0^{d/2} F(r)\, 2\pi r\, dr}{\int_0^{\infty} F(r)\, 2\pi r\, dr} \tag{1}$$

The intercept diameter d is proportional to the dish diameter D for a given receiver temperature. The optical efficiency is therefore determined by the receiver temperature, and is insensitive to scaling of the dish size. The collected power then scales with the dish aperture area.

$$P_{COLL} = \frac{\pi D^2}{4} I_{DN} \cdot \rho\ \eta_{INT} \tag{2}$$

A more detailed analysis might also account for shading, if a large size heat rejection surface or secondary reflector is used; and for losses in additional optical stages, if a secondary concentrator or a Cassegrainian configuration is used.

2.2 Receiver. Conventional receivers for large-scale solar thermal electricity generation systems are usually stand-alone devices, connected to a nearby heat engine via pipes carrying the heated fluid. This approach cannot be used in a micro-scale device, since the bulk and cost of the thermal insulation needed to prevent thermal losses to the environment will be excessive. We, therefore, propose a different approach that is adapted to micro-scale conversion systems, essentially eliminating the need for thermal insulation.

We presume that the micro-scale generators considered here (Section 2.3) have the general shape of thin rectangular boxes. In all cases except the Brayton engine, the two larger faces of the box are used as the hot and cold heat exchangers. The proposed receiver is made of a rectangular cavity, as shown in Fig. 2*a*. Five sides of the cavity are formed from integral units comprising each of a solar absorber, a generator, and a heat rejection element. The last side of the cube is a front plate containing the aperture for incident concentrated solar radiation.

The solar absorber, serving also as the high-temperature heat sink of each generator, can be enhanced to increase absorptivity with surface roughness or an extended surface produced, e.g., by parallel grooves. The choice of material depends on the temperature range, and experience from large-scale solar receivers can help identify suitable materials. For example, Silicon Carbide has an attractive combination of mechanical and thermal stability over a wide temperature range, and good absorptivity; it was also proposed as a structural material for the miniature Brayton generator [8]. The external side of the receiver/generator is composed of extended surface heat sinks that reject low-temperature heat to the environment (Section 2.3). Since the receiver's external walls are composed of these heat rejection elements, and the hot receiver surfaces have no direct connection to the environment, there is no need for insulation of the receiver cavity.

Optionally, the receiver cavity formed by the generators and the front plate may be closed with a transparent window at the aper-

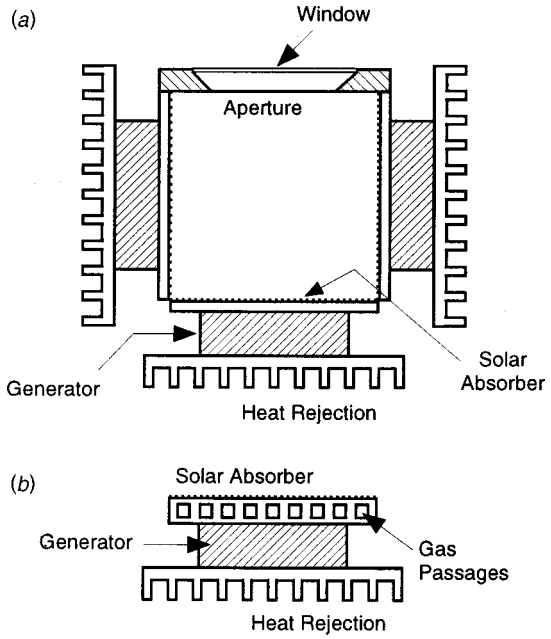

Fig. 2 ***a*) Structure of the STIMGen receiver/generator, the shown window is optional; *b*) Solar absorber containing internal passages for Brayton cycle heat exchange and for hybrid operation; the heat exchanger passages may be channels (as shown), or another microstructure that provides enhanced heat transfer area.**

ture, as shown in Fig. 2*a*, and filled with a relatively inert gas such as nitrogen. This can prevent oxidation or other damage to the absorber surfaces, and considerably reduce the convection and emission losses through the aperture. Appropriate window materials such as fused silica are transparent over the entire solar spectrum, and can withstand relatively high temperature without adverse effects [9].

The efficiency of the receiver is calculated by evaluating the various losses. The emission loss is estimated by assuming that the cavity is equivalent to a black surface with area equal to the area of the aperture A, and temperature equal to the average temperature T_{HS} of the internal absorber surfaces. Convection loss through the aperture is estimated using an algorithm for high temperature cavities [10], which is quite complex and will not be reproduced here. Conduction loss is not present in its usual sense, since the absorbing surfaces do not have an interface to the ambient. Conduction through the generator to the cold side is accounted for separately (Section 2.3). The receiver efficiency is then:

$$\eta_R = 1 - \frac{A\sigma T_{HS}^4 + P_{CONV}}{P_{COLL}} \tag{3}$$

A more detailed analysis might also account for the effects on non-uniformity in the distributions of incident flux and temperature on the receiver surfaces.

2.3 Electricity Generation. Several options are available for generating electricity on small scale, using existing or emerging technologies. These generators are in principle exchangeable, since they all can be viewed as a black box with heat input, heat rejection, and appropriate flow and electric connections. Obviously, this is a simplistic view since a system needs to be optimized separately for each specific generator technology. However, it is noteworthy that the principles are similar. Four options are presented in this section: two heat engines (Stirling and Brayton) and two direct converters (thermoelectric and thermophotovoltaic). The first two options will be analyzed in some detail.

Size Scaling. In a standard thermodynamic analysis of power cycles, the device size and its power level are usually scaled out and the analysis deals only with efficiency and specific power. However, for small-scale devices this does not hold, due to a significant size-dependent power loss that is usually neglected in large-scale devices. Heat is conducted through the generator's structure, bypassing the energy conversion process (this is sometimes called *thermal shunt* loss). This loss depends on the physical size of the engine, and not only on the thermodynamic variables [11,12]. This power lost by conduction is proportional to the generator size:

$$P_{COND} = k_G R_{COND} D_G^2 (T_{HS} - T_{LS})/R_H D_G \propto D_G \tag{4}$$

The power produced in a heat engine is usually proportional to the displaced volume in the engine. If the engine is scaled geometrically (constant R_{COND}, R_{H}), the ratio of the heat conduction loss per unit volume is indicative of the relative magnitude of this heat loss. The scaling of this ratio with generator size is:

$$\frac{P_{COND}}{P_{GEN}} \propto \frac{D_G}{D_G^3} = D_G^{-2} \tag{5}$$

Very small engines will be therefore excessively inefficient. This is a limiting factor on generator downscaling, as noted for Stirling engines by [12].

In a solar device, the scaling of generated power relative to system size is different. The heat input to the generator, and therefore the generated power, is determined by the incident radiation that scales with D^2, according to Eq. (2). One way to satisfy this constraint is to vary the generator size not in proportion to the dish size, but following the relation $D_G^3 \propto D^2$. However, this implies that as we scale down the system, the generator becomes large relative to the dish. Another way to satisfy the scaling imposed by the dish is to note that the generator power is determined not only by its size, but also by flow rate (in an open cycle) or frequency (in a closed cycle). For example, if the frequency of a Stirling engine is varied with size such that $f \cdot D_G$ is constant, then the power output can be estimated as [13]:

$$P_{GEN} \propto f \cdot D_G^3 \propto D_G^2 \tag{6}$$

The required scaling of the frequency, $f \propto D_G^{-1}$, is the same as the scaling of the natural frequency [11]. When the relation in Eq. (6) holds, the generator can be scaled down geometrically, with its linear dimension proportional to the dimension of the dish: $D_G \propto D$. The scaling of the engine conduction loss then differs from Eq. (5):

$$\frac{P_{COND}}{P_{GEN}} \propto \frac{D_G}{f \cdot D_G^3} \propto D_G^{-1} \tag{7}$$

The increase of the relative conduction loss is therefore slower in the solar-driven engine due to the need to match the scaling of the collected power. Additional degrees of freedom might be used to obtain the correct matching of the power collected by the dish to the power that can be converted by the engine. For example, the operating pressure can be varied, or several parameters (geometry, frequency, pressure) can be varied simultaneously. For the current study, we assume that the engine design is scaled to satisfy Eq. (6).

Generator Model. The models developed for this analysis are simplified; only major aspects that can be modeled without referring to the detailed design of the engine are included. The system efficiency predicted by these models may therefore be overestimated. Internal losses by conduction and radiation are included for both cycles. The Stirling cycle model includes imperfect regeneration, but not friction losses. External irreversibility due to temperature gradients at the heat sinks is modeled in some detail, since its effect on efficiency can be significant. The internal losses in the Brayton cycle were included as a global isentropic effi-

Table 1 Design parameters and assumptions for the STIMGen collector and heat engines.

Collector		**Brayton cycle**	
Dish rim angle	45°	Gas	Air
Reflectivity ρ	0.9	Compressor isentropic eff. η_C	0.75
Beam quality (mrad)	3.0	Turbine isentropic eff. η_T	0.75
Insolation (W m^{-2}) I_{DN}	800	Compression ratio R_p	3.0
Engine (general)		Fixed pressure loss L_p	8%
Height ratio R_H	0.3	Recuperator effectiveness ε_{HX}	0.9
Conduction area ratio R_{COND}	0.1	**Stirling cycle**	
Radiation area ratio R_{RAD}	0.3	Gas	helium
Engine conductivity k_G (W m^{-1} K^{-1})	1.0	Mean pressure (bar)	10.
Electrical generator efficiency η_E	0.9	Expansion ratio R_p	1.5
Ambient temperature (K)	300	Regenerator effectiveness ε_{HX}	0.9

ciency, without referring to design-specific effects such as tip leakage that can have significant size dependence. Pressure loss in the Brayton cycle due to flow through the receiver and recuperator is modeled; any additional pressure losses due to flow control, combustor, etc., are represented as a fixed fractional pressure loss.

Thermal conduction between the hot and cold side of the engine was computed using Eq. (4). An additional mechanism for heat loss is thermal radiation between the hot and cold sides of the generator. This can become significant as the temperature of the hot size increases. However, this loss is reduced by the presence of additional intermediate components serving as radiation shields. The loss of thermal energy by radiation between the engine hot and cold sides was estimated as:

$$P_{RAD}=R_{RAD}D_G^2\varepsilon\sigma(T_{HS}^4-T_{CS}^4) \tag{8}$$

The ratio of this radiative loss to the generated power is neutral to scale of the generator.

The following assumptions on the geometry and properties of the generator materials were used in the numerical results presented below. The ratio of cross section areas available for conduction and radiation to the generator's total cross-section area were estimated as $R_{COND}=0.1$ and $R_{RAD}=0.3$. The ratio of the conduction path length, or the generator's height, to its width was estimated as $R_H=0.3$, following the approximate proportions of [8]. The wall conductivity was $k_G=1.0$ W m^{-1} K^{-1}, in the middle of the feasible range of materials [12]. Some cases were compared to much lower conductivity of $k_G=0.1$ W m^{-1} K^{-1}. The emissivity of the internal surfaces was $\varepsilon=0.4$. Additional engine parameters are presented in Table 1.

Stirling Cycle. The Stirling cycle is an attractive option for power generation due to its high efficiency, theoretically reaching the Carnot limit. Practical Stirling engines often fall short of this theoretical performance, but careful design should be able to achieve a high fraction of the ideal efficiency [14]. Stirling engines are also popular in solar thermal systems, and hold the current record in solar to electricity conversion efficiency [1,15]. Small Stirling cycle engines with a traditional piston mechanism were proposed down to the scale of a few centimeters [11]. However, on a smaller scale the use of membranes rather than pistons for fluid displacement would be preferable [11,16]. Scaling to small size can improve some aspects of the engine performance, such as increasing heat transfer and reducing the effect of inertia. On the other hand, other effects are negative, such as increase of pressure loss in flow through narrow passages.

We use the simple Stirling cycle model of [12] to evaluate the generator efficiency:

$$\eta_G=\eta_S\eta_E=\frac{(\gamma-1)(\tau-1)\ln R_p}{(\gamma-1)\tau\ln R_p+(\tau-1)[1-\varepsilon_{HX}]}\eta_E \tag{9}$$

This model already includes the effect of imperfect heat transfer between the regenerator and the fluid. The regenerator effectiveness is taken as $\varepsilon_{HX}=0.9$, which is a typical value over a wide range of the internal heat transfer coefficient and heat exchanger material selection [17]. The bypass of heat by conduction and radiation from the hot side to the cold side of the engine were computed separately as described above.

A major cause of efficiency reduction is the temperature differences due to imperfect heat transfer between the gas at temperatures T_H, T_C and the hot and cold heat sinks at T_{HS}, T_{CS} [14]. Several correlations are available for the average heat transfer coefficient in a piston-cylinder system, for example [18,19]. The heat transfer coefficient derived from these correlations scales as $D_G^{0.6}$ [18] and $D_G^{1.4}$ [19], i.e., heat transfer is reduced for smaller devices; this is not acceptable for microscale heat transfer. These correlations were developed for larger systems, where the heat transfer is dominated by complex secondary flow effects. In the microscale regime, these secondary flows should be diminished, and heat transfer should be dominated by conduction and therefore improve as the device size is reduced. An alternative transient conduction model was used to determine the heat transfer at the heat sinks. The time-averaged heat transfer coefficient is given by Eq. (*A*4) in the Appendix.

An additional temperature difference exists between the cold sink and the ambient. The magnitude of the heat flux to be rejected to the environment is similar to, or even lower than, the heat flux generated by modern computer processors. The solution used in computers, a compact fin array and a small blower, could be applicable to reject heat from the micro-engines. Typical performance values for CPU coolers were used to evaluate the STIMGen heat rejection. Typical CPU heat flux is about 40 W cm^{-2}, for modern chips of die size 100–150 mm^2. The thermal resistance of the fin array unit is about 0.5°C W^{-1} cm^2. The power consumption of the blower is about 2 W for 50 W of heat removed. The thermal resistance value was used to compute the temperature difference between the cold sink and the environment at 300 K. The parasitic power was subtracted from the generator's power output.

Brayton Cycle. Large scale Brayton cycle engines (gas turbines) are a popular choice in power generation in general, as well as in solar power generation [20–22]. A miniature Brayton cycle engine is under development at MIT [8]. The engine size is about 1 centimeter in diameter, and it should be able to generate around 10 W of electricity. Such a micro gas turbine can be a candidate for integration in a STIMGen.

Efficiency of a recuperative Brayton cycle can be described by the following set of equations:

$$\begin{aligned} W_C&=\frac{1}{\eta_C}T_C(R_p^{(\gamma-1)/\gamma}-1)\\ W_T&=\eta_T T_H(1-(R_p(1-L_p))^{-(\gamma-1)/\gamma})\\ T_{RCP}&=T_C+W_C+\varepsilon_{HX}(T_H-T_C-W_C)\\ \eta_B&=\frac{W_T-W_C}{T_H-T_{RCP}} \end{aligned} \tag{10}$$

This model includes the irreversibility in the compressor and turbine, incomplete recuperation, and pressure losses due to the combustor, recuperator and solar receiver. Table 1 shows the values used for the cycle parameters. The additional power losses due to heat conduction and radiation through the engine structure are calculated separately following Eqs. (4) and (8).

Heating of the working gas between the recuperator and the turbine is accomplished in a heat exchanger embedded within the hot sink as shown in Fig. 2*b*. The gas enters the hot sink after leaving the recuperator at temperature T_{RCP} and exits at T_H. T_H is found by solving the energy balance equation:

$$\dot{m}C_p(T_H - T_{RCP}) = hA_{channel}\frac{(T_{HS}-T_H)-(T_{HS}-T_{RCP})}{\ln\dfrac{(T_{HS}-T_H)}{(T_{HS}-T_{RCP})}} \tag{11}$$

The convection coefficient h and the pressure drop can be found from well-known relations for laminar flow and heat transfer in rectangular ducts. The flow is expected to be laminar since the width of the channels in the heat exchanger are of millimeter size or less; computed values of the Reynolds number justify this assumption. The channel aspect ratio can affect the friction factor and the Nusselt number, and representative values that correspond to aspect ratio of 2.5 are used:

$$f\cdot \mathrm{Re}_D = 65$$

$$Nu_D = \frac{hD_h}{k} = 3.7 \tag{12}$$

where Re_D and Nu_D are based on the channel's hydraulic diameter D_h. The pressure loss in the heat exchanger channels according to the friction factor of Eq. (12) was added to the fixed pressure loss (Table 1) as an additional penalty on performance. The channel dimensions in the hot sink heat exchanger were optimized to provide the highest system efficiency. The additional pressure loss in the recuperator is computed in the same way.

Thermoelectric Converter. Thermoelectric (TE) devices have been in use for a while, mostly for cooling applications, but they can also be used for generation of electricity from heat. The main advantage of TE over heat engines is the lack of moving parts hence greater reliability. On the other hand, TE currently has lower efficiency than heat engines, about 10% of the Carnot limit. Due to the low efficiency, TE has not been very popular in solar energy [23] or for power generation in general.

The low efficiency is due to the properties of currently available materials, and there does not seem to be a fundamental reason why TE devices cannot attain higher efficiency [24]. New approaches to TE materials promise significant improvements in the near future [25]. In addition, most TE devices operate at relatively low temperatures; increasing the temperature will increase the device's efficiency. With proper choice of materials, operation at over 800 K may be considered [26]. The combination of new materials and high-temperature operation could bring TE generators to an efficiency level comparable to photovoltaic cells or heat engines. If this is realized, then TE generators will become significant contenders for a STIMGen system, with the inherent advantages of simplicity and reliability when compared to heat engines. A related option that can operate at high temperature and may achieve higher efficiency is a two-stage thermionic/thermoelectric conversion process [27].

Thermo-Photovoltaic Converters. High temperature thermophotovoltaic (TPV) converters have been developed and demonstrated on a kilowatt scale. Similar to TE generators, TPV generators have no moving parts and should have greater reliability than heat engines. TPV currently has lower efficiency than heat engines, in the range 5–10% from heat to electricity; however, higher conversion efficiency up to 20% should be possible [28]. Current limitations are related to material properties. A good TPV system requires a selective emitter/filter system with well-defined transmission band and low absorption losses; and a PV cell with a bandgap that is well matched to the transmission band of the filter. If such a combination can be realized in an appropriate wavelength, for example around 1.5 μm, corresponding to emitter temperature of 1,400°C [29], then a competitive TPV-STIMGen system may be realized. In this system, the selective emitter is the back face of the solar absorber, and the PV cell is attached to the back of the external heat sink. A minimal mechanical support completes the simple generator unit, with no need for pressure sealing (as for the heat engines) and no need for thermal insulation.

2.4 Hybridization. Operation of a thermal plant can continue even when sunlight is not available by supplying heat from an alternative source. Heat from conventional fuel can be supplied to a STIMGen by attaching a small external combustion unit to the receiver/generator assembly, or by integrating the combustion unit within the generator [8]. The fuel should be a clean-burning and easily distributed fuel such as hydrogen or methane. For the Brayton cycle, a combustor and heat exchanger are already integral parts of the system. For the Stirling generator and the direct converters, a heat exchanger as shown in Fig. 2*b* can be inserted at the absorber, similar to the Brayton STIMGen. Hot air from the combustion chamber is guided into the internal channels to heat the high-temperature heat sink. When sunlight becomes available, this flow can be reduced or stopped. If the heat exchanger is made from a material having high specific heat, then it can also serve as short-term thermal storage that will smooth any transients in the heating processes.

Including a combustor in a STIMGen poses several additional challenges to the system design. Miniature combustors are a technology currently under development. A fuel distribution system, flow control, and recuperation add to the complexity and cost of the system. These difficulties may be alleviated if some of the needed components (such as controls and heat exchangers) can be integrated into the generator structure and, therefore, manufactured simultaneously with little added cost. Additional design and experimentation are needed to determine which solutions can be practical and cost-effective for small-scale distributed combustion.

3 Results

Since the two direct conversion systems that were described above currently have relatively low efficiency, we present here only results for the two heat engine options.

3.1 Stirling Cycle STIMGen. The efficiency of a Stirling-based STIMGen as a function of temperature is presented in Fig. 3*a*, for two sizes of the primary collector. The engine size is about 0.015 m and 0.03 m for dish diameter of $D=0.5$ m and 1.0 m, respectively. The variation of efficiency with temperature shows a maximum, due to the opposing effects of temperature variation, as seen in Fig. 3*b*. The magnitude of the external irreversibility due to temperature drops at the heat sinks is diminished as the temperature increases, leading to higher engine efficiency. This can be seen in the variation of the relative loss of temperature potential, $1-(T_H-T_C)/(T_{HS}-T_{CS})$, which is reduced at higher temperature. On the other hand, the receiver losses and the heat bypass inside the engine increase with temperature. The maximum efficiency is about 30 percent at 1,000 K for the 0.5 m dish, and 27% at 1,100 K for the 1.0 m dish.

The dependence of system efficiency on size at fixed receiver temperature of 1,100 K is shown in Fig. 4*a*. Optimal performance is obtained around $D=0.7$ m (generator size 0.019 m), where the system solar-to-electricity efficiency is 29 percent. The efficiency for lower generator conductivity of 0.1 W m^{-1} K^{-1}, at the lower limit of feasible material properties [12], is also shown for comparison. The trend is similar, but the efficiency optimum is higher (36%) and is shifted to smaller dish size of 0.34 m (generator size

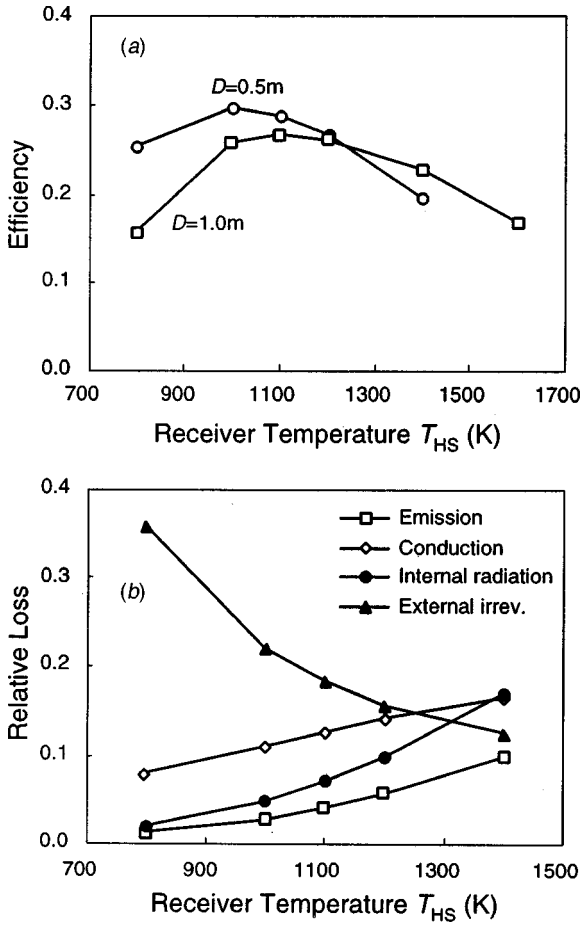

Fig. 3 System performance of a Stirling STIMGen as a function of receiver temperature: *a*) Total efficiency from radiation to electricity for dish diameter of 0.5 m and 1 m; *b*) Dominant loss mechanisms for $D=0.5$ m: receiver emission, engine internal conduction, and internal radiation are normalized to the collected radiation power; external irreversibility is defined as $1-(T_H-T_C)/(T_{HS}-T_{CS})$.

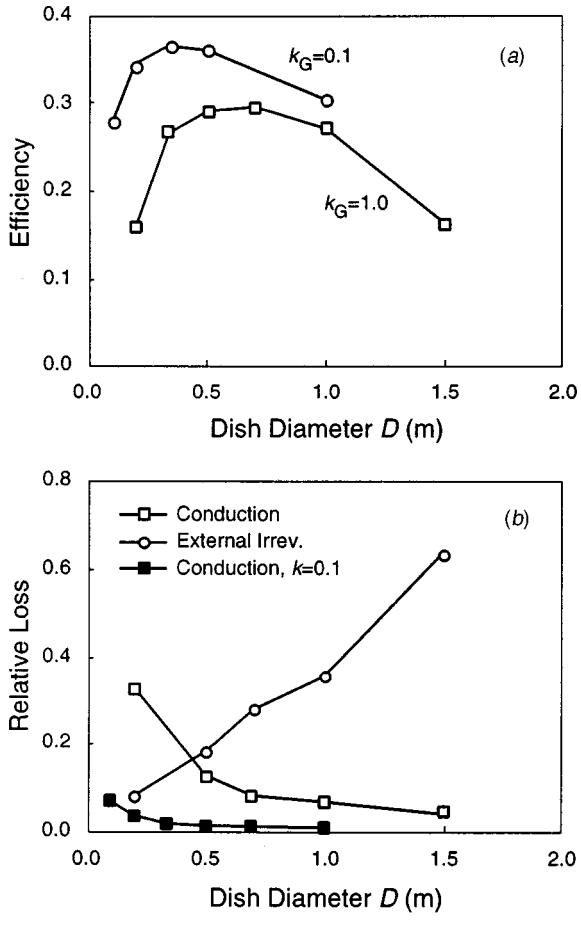

Fig. 4 System performance of a Stirling STIMGen as a function of dish diameter: *a*) Total efficiency from radiation to electricity for receiver temperature of 1,100 K, and generator conductivity of 0.1 and 1.0 W m^{-1} K^{-1}; *b*) Dominant loss mechanisms for $T=1{,}100$ K: engine internal conduction is normalized to the collected radiation power; external irreversibility is defined as $1-(T_H-T_C)/(T_{HS}-T_{CS})$.

0.010 m). The main loss mechanisms are shown in Fig. 4*b*. The loss due to generator conduction increases as the size decreases, approximately following the scaling of Eq. (7). On the other hand, heat transfer at the heat sinks improves as the size decreases, and therefore the external irreversibility is reduced. The temperature differences from the heat sinks to the gas decrease, increasing the gas temperature ratio T_H/T_C and therefore increasing the internal cycle efficiency. These opposing trends create an optimal system size. For the lower conductivity case, the conduction loss is much smaller, and a significant increase of this loss occurs only at dish size below 0.2 m, compared to 0.5 m for the higher conductivity. This permits much smaller systems to remain efficient, as shown in Fig. 4*a*. The other loss components are relatively insensitive to the size variation and do not play a significant role in the optimization of system size.

3.2 Brayton Cycle STIMGen. The performance of a Brayton-based STIMGen is presented in Fig. 5. The general trends are similar to the Stirling STIMGen. Variation of the total efficiency with temperature, Fig. 5*a*, shows an optimal temperature, again due to the balance between two effects. The engine's internal efficiency improves with higher temperature, but the external losses (receiver and generator thermal shunt) also increase. The maximum system efficiency of 13.3% is at temperature of 1,200 K for dish diameter of 0.5 m, and 14.6% at 1,300 K for dish diameter of 1 m. These are significantly lower than the corresponding maximum values for the Stirling systems, and the optimum occurs at higher temperatures for the same system size.

The variation of system efficiency with size is shown in Fig. 5*b* for a fixed receiver temperature of 1,200 K. Similar to the Stirling model described above, we find an optimal size for a Brayton-based STIMGen. This is again due to the balance between the internal conduction loss, which becomes significant at smaller system size, and the external irreversibility due to heat transfer, which dominates at the larger size. The optimal collector size is $D=0.7$ m (generator size 0.019 m), with system efficiency of 14.5% which is about half of the corresponding Stirling STIMGen.

The size dependence of the system efficiency is shown also in Fig. 5*b* for generators with a lower thermal conductivity of 0.1 W m^{-1} K^{-1}. The trend is similar, with higher efficiency values and an optimum of 16.4% shifted to smaller system size of $D=0.5$ m. This shift is similar to the Stirling STIMGen and is due to the reduction in conduction loss, which begins to increase only at smaller system size and, therefore, permits smaller systems to remain efficient.

4 Discussion

A new approach was proposed for the integration of solar thermal conversion devices, where the basic unit is as small as pos-

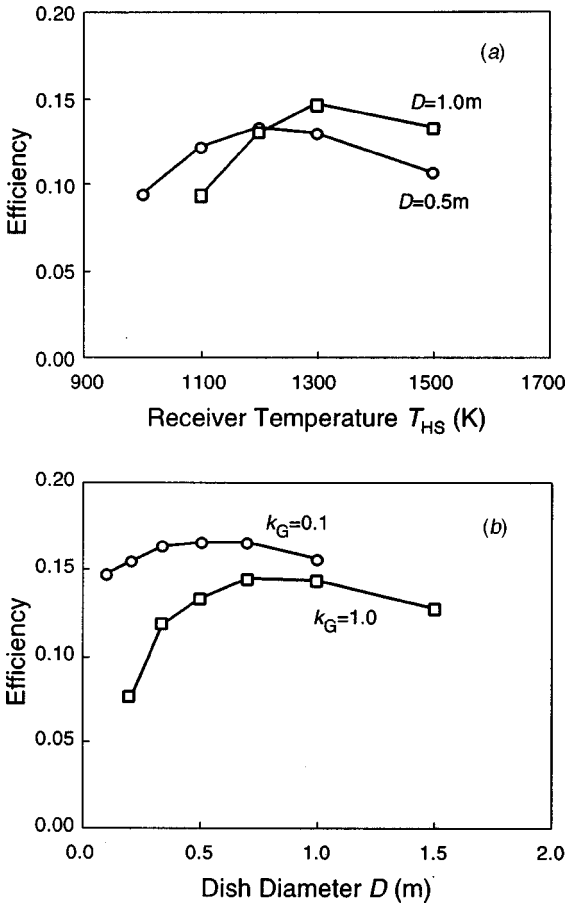

Fig. 5 System performance of a Brayton STIMGen: *a*) Total efficiency from radiation to electricity as a function of receiver temperature for dish diameter of 0.5 m and 1 m; *b*) Total efficiency from radiation to electricity as a function of dish size for receiver temperature of 1,200 K, and generator conductivity of 0.1 and 1.0 W m^{-1} K^{-1}.

sible rather than as large as possible. The most attractive option, based on efficiency estimates, is a STIMGen based on Stirling cycle generators. Predicted system efficiency was about 30% at the best size and operating temperature. The other options are significantly less efficient, but future advances may help reduce the gap in performance potential. We found that the preferred scale of a STIMGen is a collector diameter of about 0.5–1 m, and generator size of about 1 cm. This is based on efficiency estimates; a refinement of the efficiency estimates, and addition of other considerations such as cost, manufacturing processes etc., can modify this preferred size. The proposed approach of an integral structure for the thermal and generation functions can be used in a solar device, and can be also effective in a device where heat is provided from conventional or renewable fuel.

Theoretical models tend to over-predict the efficiency for Stirling cycles, so the present results should be considered with caution. However, even if we presume that a real STIMGen device will show only half the efficiency of the theoretical model, efficiency values of around 15% are quite attractive compared to existing solar energy conversion systems. Typical efficiency values of solar generators (both photovoltaic and thermal) are in the range of 10–20%. The highest recorded efficiency of a macroscale solar generator was 29%, achieved, quite appropriately, with a Stirling engine [15]. This demonstrates the potential of Stirling-based systems to provide very effective conversion of solar energy, and the potential of a Stirling-based STIMGen to compete with some larger systems.

The predicted efficiency of a recuperated Brayton system was about 15%, comparable to current commercial photovoltaic cells, and to current large-scale solar thermal systems such as parabolic trough or Rankine-based power towers. As in a Stirling engine, there will be a difference between the model results and a real system, but we have anticipated some of this difference by choosing conservative values for the component efficiencies and internal pressure drop. The performance of a real Brayton STIMGen might, therefore, be close to the model prediction, which would make it still a reasonable contender compared to other solar converter options.

Stirling engines that were previously used in larger-scale solar energy systems [15] required large and expensive heat exchangers, and suffered from reliability problems. Both problems may be alleviated in a STIMGen. Heat transfer from the hot sink to the internal fluid in the engine improves at smaller sizes, as seen in our results and in other studies [11]. The heat exchanger is, therefore, more compact and temperature differences are smaller. Reliability might be improved if a membrane-based rather than piston-based engine can be developed, and the engine will then operate essentially without moving parts (in the sense of sliding contact).

The high efficiency provided by the Stirling cycle can be used with any high-temperature heat source, not just with solar heat. Heat derived from combustion of conventional fuel or biomass will be converted at the generator efficiency, which is higher than the solar plant efficiency since optical and receiver losses are absent. For example, the predicted heat to electricity conversion efficiency is 37% or 46% for the optimal generator with conductivity of 1.0 or 0.1 W m^{-1} K^{-1}. These values do not include losses in the heat supply system, such as stack losses or blower parasitic power consumption. Again, even if we assume that the efficiency of a real device will be about half of the theoretical model prediction, the result is still comparable to much larger engines that are in use today at power levels of 10–100 kW. A non-solar TIMGen (Thermal Integral Micro Generator) can be constructed from six generators as a rectangular cavity similar to Fig. 2, again to avoid excessive losses from the hot surfaces and avoid the need for thermal insulation. The internal cavity can be designed to serve as the combustion chamber and heat exchanger that supplies heat to all six generators.

It is not currently possible to predict the actual cost of a mass-produced STIMGen. MEMS technology in general is still experimental, and there is insufficient experience in mass production of MEMS components and systems. High-temperature MEMS is even less developed and more difficult to predict. The only qualitative statement that can be made is based on experience of other industries where mass production has led to significant cost reduction down to a competitive level. The small system size provides a rapid transition to mass production scale, as compared to large-scale plants. For example, the Stirling STIMGen at $D = 0.5$ m and $T_{HS} = 1{,}100$ K produces 45 W of electricity under nominal conditions. For a total capacity of 100 MW_e, the number of STIMGen dishes and individual generators will be about 2 million and 10 million, respectively. In comparison, for a centralized solar generation scheme, this capacity represents a single custom-built system, and many similar plants are required before mass production can be contemplated.

Several application areas can be considered for STIMGen devices. The first will probably be remote off-grid small systems, where the cost of fuel supply for conventional generators is very high, and therefore, the value of electricity is high enough to justify innovative technology. Currently the only solution for this market is photovoltaic panels, which are expensive and cannot be hybridized. If STIMGen technology is successful in this niche, then eventual improvements in performance and cost may justify its penetration into the bulk electricity market. Modularity and access to mass production should be the main aspects driving the use of STIMGen systems in this more competitive field. Another

kind of application that may be considered is portable power, if a design for a folding concentrator can be made that will be accurate and reliable enough to drive the high-temperature receiver.

Parts of the technology for construction of STIMGen systems already exists today, while other parts are currently under development. Most likely, the first systems constructed will not yet operate at the high efficiency levels that were predicted here. Further development is needed in several aspects: the integral receiver/heat exchanger, miniature heat engine technology, miniature combustors, and new materials for the direct generators. The promise of modular, scalable, mass-produced, and eventually efficient, hybrid solar generators justifies this effort.

Nomenclature

A = Area of the receiver aperture (m^2)
C_p = Specific heat ($J\,kg^{-1}\,K^{-1}$)
d = Diameter of the receiver aperture (m)
D = Parabolic dish diameter (m)
D_G = Width of the generator (m)
D_h = Hydraulic diameter (m)
f = Stirling engine frequency
F = Incident flux ($W\,m^{-2}$)
h = Heat transfer coefficient ($W\,m^{-2}\,K^{-1}$)
I_{DN} = Direct normal insolation ($W\,m^{-2}$)
k = Thermal conductivity of the gas ($W\,m^{-1}\,K^{-1}$)
k_G = Thermal conductivity of the generator's wall ($W\,m^{-1}\,K^{-1}$)
L_p = Fractional pressure loss in a Brayton cycle
P_{COLL} = Power collected into the receiver aperture (W)
P_{COND} = Power lost by conduction between the two sides of the generator (W)
P_{CONV} = Power lost by convection from the receiver aperture (W)
P_{RAD} = Power lost by radiation between the two sides of the generator (W)
P_{GEN} = Power generated (W)
q = Heat flux ($W\,m^{-2}$)
R_p = Compression ratio
R_{COND} = Ratio of conduction area to total generator cross-section area
R_{RAD} = Ratio of area free for radiation to total generator cross-section area
R_H = Ratio of generator's height to width
T_H, T_C = Hot and cold gas temperatures (K)
T_{HS}, T_{CS} = Hot and cold heat sink temperatures (K)
T_{RCP} = Recuperator exit temperature (K)
W_T, W_C = Specific work at the turbine and compressor of a Brayton cycle (K)

Greek

γ = Ratio of specific heats
ε = Emissivity
ε_{HX} = Regenerator effectiveness (Stirling cycle), Recuperator effectiveness (Brayton)
η_B, η_S = Brayton, Stirling cycle efficiency
η_C, η_T = Compressor and turbine isentropic efficiency (Brayton cycle)
η_E = Work to electricity conversion efficiency
η_G = Generator efficiency
η_{INT} = Intercept efficiency
ρ = Reflectivity
σ = Stefan-Bolzmann constant, $5.669\cdot10^{-8}\ W\,m^{-2}\,K^{-4}$
τ = Ratio of gas temperatures: $\tau = T_H/T_C$

Appendix: Heat Transfer at the Stirling Heat Sinks

For small device sizes, the heat transfer between the cylinder and the gas in a piston-cylinder system is likely to be dominated by conduction in the gas. Convective effects such as swirl, which dominate in large cylinders, are expected to play only a secondary role. The problem is modeled as a volume of gas that expands following the piston in simple axial plug flow. Heat is transferred from the end of the cylinder to the gas by conduction only. The parameters used to estimate the conduction process are the average gas temperature and the distance from the cylinder head to the middle of the gas space (lumped parameter analysis). Following the ideal Stirling cycle, the speed of the piston is controlled to keep the process isothermal, such that the cylinder temperature and the average temperature of the gas are constant.

The change in internal energy during the expansion is zero since the gas average temperature is constant. The heat transferred to the gas is therefore converted completely to work in the piston. The work done on the piston as it moves a small distance dx from its current position x is:

$$\delta W = p\,A\,dx = \frac{mRT_H}{V}A\,dx = mRT_H\frac{dx}{x} \tag{A1}$$

A is the piston cross-section area, p is the gas pressure, V is the gas volume, m is the mass of the gas in the cylinder, and R is the gas constant. The heat flux through the cylinder head is given by the temperature difference and the distance between the cylinder head and the middle of the gas volume:

$$\delta Q = qA\,dt = kA\frac{T_{HS}-T_H}{x/2}dt \tag{A2}$$

Combining Eqs. (*A*1) and (*A*2), the solution for the piston displacement and heat flux can be found:

$$x(t) = x_0 + \frac{2kA(T_{HS}-T_H)}{mRT_H}t \equiv x_0 + \dot{x}t$$

$$q(t) = \frac{2k(T_{HS}-T_H)}{x_0+\overline{x}t} \tag{A3}$$

x_0 is the minimum clearance position of the piston. The time required for the piston to reach full stroke $x(\tau) = x_0 + s$ is: $\tau = s/\dot{x}$. The average heat flux during this period and the average heat transfer coefficient are then:

$$\overline{q} = \frac{1}{\tau}\int_0^\tau q(t)dt = \frac{2k(T_{HS}-T_H)}{s}\ln\left(1+\frac{s}{x_0}\right)$$

$$\overline{h} = \frac{\overline{q}}{T_{HS}-T_H} = \frac{2k}{s}\ln\left(1+\frac{s}{x_0}\right) \tag{A4}$$

This model is conservative since it does not include heat transfer through the sidewalls, and neglects any enhancement that may exist due to non-plug flow effects (secondary flow that promotes mixing). On the other hand, conventional Stirling machines usually employ sinusoidal motion and do not attempt to control the piston such that isothermal conditions are preserved. However, since inertia effects diminish in the microscale [11], it may be feasible to control the piston motion and approach the ideal process.

References

[1] Winter, C.J., Sizmann, R.L., and Vant-Hull, L.L., 1991, *Solar Power Plants*, Springer-Verlag, Berlin.
[2] Becker, M., and Klimas, P.C., 1993, *Second Generation Central Receiver Technologies*, Verlag C. F. Müller, Karlsruhe.
[3] Majumdar, A., and Tien, C.L., 1998, "Micro Power Devices," Microscale Thermophys. Eng., **2**, pp. 67–69.
[4] Feuermann, D., and Gordon, J.M., 1998, "Solar Fiber-Optic Mini-Dishes: A New Approach to the Efficient Collection of Sunlight," Sol. Energy, **65**, pp. 159–170.
[5] Cariou, J.M., Dugas, J., and Martin, L., 1982, "Transport of Solar Energy with Optical Fibers," Sol. Energy, **29**, pp. 397–406.
[6] Kribus, A., Zik, O., and Karni, J., 2000, "Optical Fibers and Solar Power Generation," Sol. Energy, **68**, pp. 405–416.
[7] Zik, O., Karni, J., and Kribus, A., 2000, "The TROF (Tower Reflector Optical

Fibers) Cncept: A New Degree of Freedom for Solar Energy Systems,'' Sol. Energy, **67**, pp. 13–22.
[8] Epstein, A.H., Senturia, S.D., Al-Midani, O., Anathasuresh, G., Ayon, A., Breuer, K., Chen, K.S., Ehrich, F.F. et al., 1997, ''Micro Heat Engines, Gas Turbines, and Rocket Engines–The MIT Microengine Project,'' *28 AIAA Fluid Dynamics Conf.*, AIAA 97-1773.
[9] Karni, J., Kribus, A., Ostraich, B., and Kochavi, E., 1998, ''A High-Pressure Window for Volumetric Solar Receivers,'' ASME J. Sol. Energy Eng., **120**, pp. 101–107.
[10] Liebfried, U., and Ortjohann, J., 1995, ''Convective Heat Loss from Upward and Downward-Facing Cavity Solar Receivers: Measurements and Calculations,'' ASME J. Sol. Energy Eng., **117**, pp. 75–84.
[11] Nakajima, N., Ogawa, K., and Fujimasa, I., 1989, ''Study on Microengines: Miniaturizing Stirling Engines for Actuators,'' Sens. Actuators, **20**, pp. 75–82.
[12] Peterson, R.B., 1998, ''Size Limits for Regenerative Heat Engines,'' Microscale Thermophys. Eng., **2**, pp. 121–131.
[13] West, C.D., 1986, *Principle and Applications of Stirling Engines*, Van Nostrand Reinhold, New York.
[14] Walker, G., Fauvel, O.W., Reader, G., and Bingham, E.R., 1994, *The Stirling Alternative*, Gordon and Breach, Yverdon, Switzerland.
[15] Stone, K.W., Lopez, C.W., and Mcalister, R.E., 1995, ''Economic Performance of the SCE Stirling Dish,'' ASME J. Sol. Energy Eng., **117**, pp. 210–214.
[16] Bowman, L., Berchowitz, D.M., and Urieli, I., 1995, Microminiature Stirling Cycle Cryocoolers and Engines, U.S. Patent 5,457,956.
[17] Peterson, R.B., 1999, ''Numerical Modeling of Conduction Effects in Microscale Counterflow Heat Exchangers,'' Microscale Thermophys. Eng., **3**, pp. 17–30.
[18] Adair, R.P., Qvale, E.B., and Pearson, J.T., 1972, ''Instantaneous Heat Transfer to Cylinder wall in Reciprocating Compressors,'' *Purdue Compressor Technology Conf.*, Lafayette, Purdue Research Foundation, pp. 521–526.
[19] Chen, K., and Karim, G.A., 1998, ''Evaluation of the Instantaneous Unsteady Heat Transfer in a Rapid Compression-Expansion Machine,'' Proc. Inst. Mech. Eng., **212**, pp. 351–362.
[20] Kribus, A., Zaibel, Z., Segal, A., Carey, D., and Karni, J., 1998, ''A Solar-Driven Combined Cycle Plant,'' Sol. Energy, **62**, pp. 121–129.
[21] Romero, M., Marcos, M.J., Baonzas, F., and Fernandez, V., 1999, ''Distributed Power from Solar Tower Systems: A MIUS Approach,'' *ISES 1999 Solar World Congress*, Jerusalem, **1**, pp. 286–295.
[22] Buck, R., Heller, P., and Koch, H., 1996, ''Receiver Development for a Dish-Brayton System,'' *ASME Int. Solar Energy Conf.*, pp. 9–96.
[23] Omer, S.A., and Infield, D.G., 2000, ''Design and Thermal Analysis of a Two Stage Solar Concentrator for Combined Heat and Thermoelectric Power Generation,'' Energy Convers. Manage., **41**, pp. 737–756.
[24] Disalvo, F.J., 1999, ''Thermoelectric Cooling and Power Generation,'' Science, **285**, pp. 703–706.
[25] Dresselhaus, M.S., Dresselhaus, G., Sun, X., Zhang, Z., Cronin, S.B., and Koga, T., 1999, ''The Promise of Low-Dimensional Thermoelectric Materials,'' Microscale Thermophys. Eng., **3**, pp. 89–100.
[26] Helmers, L., Müller, E., Schilz, J., and Kaysser, W.A., 1998, ''Graded and Stacked Thermoelectric Generators–Numerical Description and Maximisation of Output Power,'' Mater. Sci. Eng., B, **56**, pp. 60–68.
[27] Naito, H., Kohsaka, Y., Cooke, D., and Arashi, A., 1996, ''Development of a Solar Receiver for a High-Efficiency Thermionic/Thermoelectric Conversion System,'' Sol. Energy, **58**, pp. 191–195.
[28] Coutts, T.J., 2001, ''An Overview of Thermophotovoltaic Generation of Electricity,'' Sol. Energy Mater. Sol. Cells, **66**, pp. 443–452.
[29] Schubnell, M., Benz, P., and Mayor, J.C., 1998, ''Design of a Thermophotovoltaic Residential Heating System,'' Sol. Energy Mater. Sol. Cells, **52**, pp. 1–9.